INSTITUTE OF PHYSICS PUBLISHING MODELLING AND SIMULATION IN MATERIALS SCIENCE AND ENGINEERING

Modelling Simul. Mater. Sci. Eng. **12** (2004) S445–S459 PII: S0965-0393(04)74402-2

First principles force field for metallic tantalum

Alejandro Strachan[1,4], Tahir Çağın[1], Oğuz Gülseren[2], Sonali Mukherjee[2,3], Ronald E Cohen[2,3] and William A Goddard III[1,5]

[1] Materials and Process Simulation Center, Beckman Institute (139-74), California Institute of Technology, Pasadena, CA 91125, USA
[2] Geophysical Laboratory and Center for High Pressure Research, Carnegie Institution of Washington, 5251 Broad Branch Road, NW, Washington, DC 20015, USA
[3] Seismological Laboratory, California Institute of Technology, Pasadena, CA 91125, USA

Received 5 October 2003
Published 10 June 2004
Online at stacks.iop.org/MSMSE/12/S445
doi:10.1088/0965-0393/12/4/S10

Abstract

We develop a many-body force field (FF) for tantalum based on extensive *ab initio* quantum mechanical (QM) calculations and illustrate its application with molecular dynamics (MD). As input data to the FF we use *ab initio* methods (LAPW-GGA) to calculate: (i) the zero temperature equation of state (EOS) of Ta for bcc, fcc, and hcp crystal structures for pressures up to ∼500 GPa, and (ii) elastic constants. We use a mixed-basis pseudopotential code to calculate: (iii) volume-relaxed vacancy formation energy also as a function of pressure. In developing the Ta FF we also use previous QM calculations of: (iv) the EOS for the A15 structure; (v) the surface energy bcc (100); (vi) energetics for shear twinning of the bcc crystal. We find that, with appropriate parameters, an embedded atom model FF (denoted as qEAM FF) is able to reproduce all this QM data. We illustrate the use of the qEAM FF with MD to calculate such finite temperature properties as the melting curve up to 300 GPa and thermal expansivity in a wide temperature range. Both our predictions agree well with experimental values.

1. Introduction

Despite decades of experimental and theoretical research on the mechanical properties of materials many questions remain open, particularly regarding the relation between atomistic processes (involving dislocations, grain boundaries, cracks, etc) and the macroscopic behaviour (plastic deformation, failure, etc). Macroscopic plasticity and failure are well characterized experimentally and described using a variety of mesoscale and macroscale models with parameters usually obtained empirically. These models and their parameters should ultimately be derivable in terms of the fundamental physics of atomic interactions as described by quantum

[4] Present address: Los Alamos National Laboratory, Los Alamos, NM 87545, USA.
[5] Author to whom any correspondence should be addressed.

mechanics. Unfortunately, despite the enormous progress in *ab initio* quantum mechanics, such calculations are too computationally demanding to study directly most processes relevant to plasticity and failure. In order to bridge this gap between atomic interactions and the mechanical properties of macroscopic systems we use extensive quantum mechanical (QM) data to derive a force field (FF) with which energies and atomic forces can be calculated in a computationally efficient way. This allows us to use classical molecular dynamics (MD) to simulate the various atomistic processes governing the mechanical and thermodynamical properties of materials. We illustrate this procedure for Ta.

Several authors have used *ab initio* methods to study mechanical properties of Ta. Söderlind and Moriarty [1] used the full potential linear muffin-tin orbital method within the GGA approximation and with spin–orbit interactions to calculate different zero temperature properties, including the equation of state (EOS) of different crystalline phases, elastic constants, and shear strength. Vacancy formation and migration energies have also been calculated from first principles [2, 3]. Also, recently, *ab initio* methods have been used to study dislocation properties in bcc metals [4].

On the other hand, several FFs have been developed for bcc metals. The first-principles-based multi-ion analytic model generalized pseudopotential (MGPT) FF has been used to calculate several mechanical and thermodynamic properties of various metals [5–7] including Ta. One of the most popular many-body FFs for metals is the embedded atom model (EAM) [8,9]. While most EAM FFs have been based on experimental data regarding structures at and near equilibrium (for bcc metals, see, e.g. [10–12]), the importance of including *ab initio* calculations of high-energy, far from equilibrium structures in developing FFs has been stressed in the past [13–16]. Very recently a new EAM potential for Ta was developed using a combination of experimental data and *ab initio* results (using the force matching method) [17]. One of the main advantages of EAM FFs is that they are computationally very efficient, which allows MD simulations of large systems for long times. The modified embedded atom model (MEAM), which includes angular dependence of the electronic density, was developed by Baskes and co-workers [18] and applied to a variety of materials including bcc transition metals [19].

In this paper, we parametrize a many-body FF (section 3) based on extensive QM calculations (section 2). We then illustrate the use of the qEAM FF with MD simulations to study various properties as a function of pressure and temperature; such as the melting curve of Ta up to pressures of $\sim$300 GPa, and thermal expansivity (sections 4 and 5). Finally, in section 6, conclusions are drawn.

2. Quantum mechanical results

We computed the static EOS of Ta for different crystalline phases using the linearized augmented plane wave (LAPW) method [20, 21]. LAPW is an all-electron method, with no essential shape approximations for the charge density or potential, and is easily converged. The 5p, 4f, 5d, and 6s states were treated as band states, and the deeper states were treated as soft core electrons. Here, we used the PBE implementation of the generalized gradient approximation [22] for the exchange-correlation potential. A $16 \times 16 \times 16$ special k-point mesh [23] was used, giving 140 k-points within the irreducible Brillouin zone of the bcc lattice. Tests demonstrated convergence with this mesh. The convergence parameter RK_{max} was 9 giving about 1800 plane-waves and 200 basis functions per atom at zero pressure.

Total energies were computed for bcc, fcc, and hcp phases at 20 volumes. For the fcc and hcp phases, $12 \times 12 \times 12$ and $16 \times 16 \times 12$ k-point meshes were used for Brillouin zone integrations giving 182 and 180 k-points within the irreducible zone, respectively. For the hcp

Table 1. EOS parameters for bcc tantalum.

	V_0 (Å^3)	B_T (GPa)	B'_T	c_{11} (GPa)	c_{12} (GPa)	c_{44} (GPa)
			Theory (0 K)			
This work (LAPW GGA)	18.33	188.27	4.08	245.18	159.8	67.58
This work (qEAM FF)	18.36	183.04	4.16	272.54	137.57	69.63
FP LMTO GGA SC[a]	17.68	203	—	281	163	93
			Theory (300 K)			
This work (qEAM FF)	18.4	176	4.9	—	—	—
			Experiment (300 K)			
Diamond Anvil cell[b]	18.04	194.7 ± 4.8	3.4	—	—	—
Ultrasonic[c]	—	—	—	266	160.94	82.47

[a] Full potential linear muffin-tin orbital calculations, Söderlind and Moriarty [1].
[b] Cynn and Yoo [26].
[c] Adiabatic elastic constants at 25°C, Katahara *et al* [28].

phase, the ideal c/a ratio was used, and c/a was optimized at two different volumes. We found that the change in the energy due to this optimization is less than 40 meV atom^{-1} around zero pressure and decreases with pressure. The energy–volume data is available as supplementary material [24]. We have fitted our energy–volume data to Rose's universal EOS [25]; the obtained zero pressure volume (V_0), zero temperature bulk modulus (B_T), and its derivative with respect to pressure (B'_T) are shown in table 1. We also show in table 1 the results obtained by Söderlind and Moriarty using a full potential linear muffin-tin orbital method within the GGA approximation and with spin–orbit interactions (denoted as FP LMTO GGA SC), and room temperature experimental values by Cynn and Yoo [26]. Our LAPW calculations of the bcc EOS agree well with the experimental values and previous theoretical calculations.

Static elastic constants ($c_s = (c_{11} - c_{12})/2$ and c_{44}) were obtained from strain energies using volume conserving tetragonal and orthorhombic deformations of the unit cell. The convergence of strain energies with respect to the Brillouin zone integration was carefully checked; we used $16 \times 16 \times 16$ k-points meshes in the full Brillouin zone giving 344 and 612 k-points within the irreducible Brillouin zone of tetragonal and orthorhombic lattices, respectively. The resulting zero pressure and zero temperature elastic constants are shown in table 1. The elastic constants c_s and c_{44} as functions of pressure [27] are available as supplementary material [24]. The zero pressure values and initial slopes are in good agreement with the experimental data of Katahara *et al* [28]. We find that c_{44} shows a change in behaviour at ∼150 GPa [27] which is probably due to the electronic transition also evident in the EOS [43]. Our results indicate that the elastic constants can be much more sensitive to changes in the occupied states below the Fermi surface than the EOS, where changes were much more subtle.

The vacancy formation energy was determined [30] using supercells of 16 and 54 atoms and a mixed-basis pseudopotential (MB–PS) code [31]. Using the GGA approximation [32], the zero pressure volume-relaxed vacancy formation energy was determined to be 3.25 eV for a 54 atom supercell, and 3.26 eV for a 16 atom supercell, indicating convergence. The effects of structural relaxation on vacancy formation energy are discussed in [30]. A comparison with recent *ab initio* and experimental results will be presented in the next section. The *ab initio* data used to calculate vacancy formation energies is also available as supplementary material [24].

3. qEAM force field

We chose to base our EAM implementation on the one proposed by Chantasiriwan and Milstein [10] because it can describe third-order elastic constants correctly. The energy of

a given atomic configuration with atom positions $\{r_i\}$ is given by

$$U\{r_i\} = \sum_{i}^{N} F(\rho_i) + \sum_{i<j} \phi(r_{ij}), \tag{1}$$

with $\rho_i = \sum_{j\neq i} f(r_{ij})$ where $F(\rho)$ is the embedding energy, ρ_i is the total 'electronic density' on the atomic site i, $f(r)$ is the electron density function, $\phi(r)$ is a two-body term and $r_{ij} = |r_i - r_j|$. Following [10] we took the two-body term to be

$$\phi(r) = \begin{cases} (r - r_m)^4 \sum_{i=0}^{7} b_i r^i & \text{if } r < r_m, \\ 0 & \text{otherwise,} \end{cases} \tag{2}$$

the factor $(r - r_m)^4$ ensures that the two-body term and its first three derivatives with respect to r vanish at the cut-off radius (r_m). The optimized form of the two-body term shows short range repulsion and longer range attraction. The 'electron density' is

$$f(r) = \frac{1 + a_1 \cos(\alpha r/V^{1/3}) + a_2 \sin(\alpha r/V^{1/3})}{r^\beta}, \tag{3}$$

where V is the volume per atom of the system. We use a cut-off radius of 9 Å for the electron density. Note that we include explicit volume dependence in $f(r)$ unlike [10]. The importance of the oscillatory behaviour of the 'electron density function' in EAM-like FFs is related to their ability to correctly account for anharmonicities [10]. Finally, following Foiles and co-workers [9] the embedding energy as a function of the electronic density is obtained from the reference bcc structure:

$$F(\rho) = U_{\text{Rose}}(V) - \sum_{i<j} \phi(r_{ij}), \tag{4}$$

where the sum is made for the perfect bcc structure and $U_{\text{Rose}}(V)$ is Rose's universal EOS [25]:

$$U_{\text{Rose}}(V) = -E_{\text{coh}}(1 + a^* + f_3 a^{*3} + f_4 a^{*4})\, \mathrm{e}^{-a^*}, \tag{5}$$

where $a^* = (a - a_0)/a_0\lambda$ and $\lambda = (E_{\text{coh}}/9V_0B_{\text{T}})^{1/2}$.

We optimized all the parameters in the qEAM FF using the following data: (a) zero temperature energy–volume and pressure–volume curves for different crystal structures (bcc, fcc, and A15) in a wide pressure range. For the bcc and fcc structures the data from section 2 were used, while for A15 we used the results obtained by Söderlind and Moriarty [1]. We also used (b) zero temperature, zero pressure elastic coefficients, shown in section 2; (c) vacancy formation energy at zero pressure; (d) energy of homogeneously sheared bcc crystal, from [1]; (e) unrelaxed (100) surface energy from [33].

We fit the parameters entering the qEAM FF energy expression to the training set using an optimization algorithm based on simulated annealing. The optimized parameters are: $r_m = 4.812\,539\,68$ Å, $b_0 = 6.502\,815\,87$, $b_1 = -11.264\,551\,30$, $b_2 = 8.014\,515\,44$, $b_3 = -2.972\,992\,23$, $b_4 = 0.600\,042\,06$, $b_5 = -0.062\,221\,06$, $b_6 = 0.002\,588\,01$, $b_7 = -0.000\,005\,04$, $a_1 = 0.072\,932\,38$, $a_2 = 0.157\,816\,72$, $\alpha = 21.796\,090\,53$ (Å^{-1}), $\beta = 7.793\,294\,26$, $a_0 = 3.323\,892\,19$ (Å), $E_{\text{coh}} = 8.154\,204\,37$ eV, $B_{\text{T}} = 183.035\,404$ GPa, $\lambda = 0.207\,827\,89$, $f_3 = -0.007\,178\,01$, $f_4 = -0.000\,005\,04$. The resulting potential functions are shown in the supplementary material [24].

A detailed comparison between the qEAM FF and the data it was fitted to is shown in the following subsections, together with other *ab initio* and experimental results.

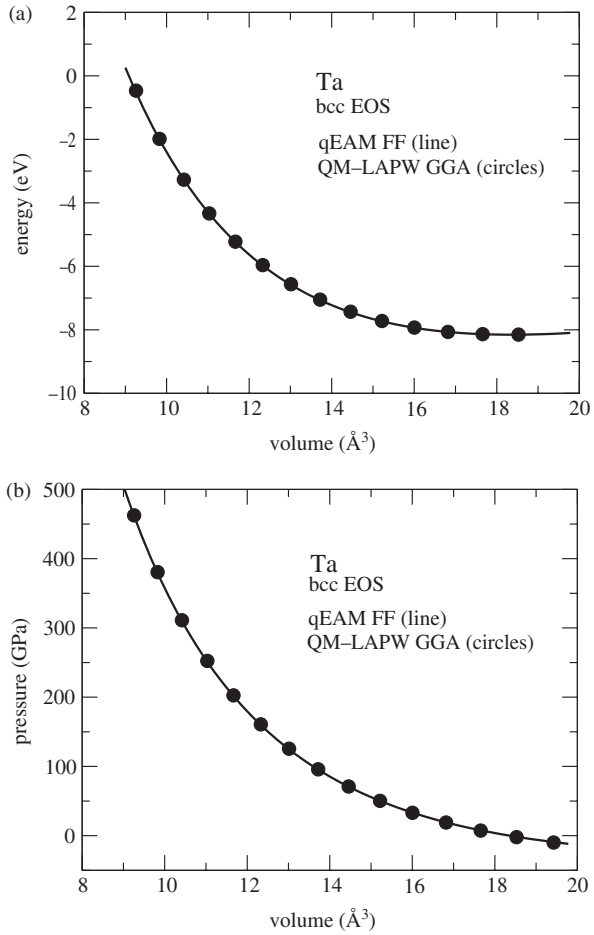

Figure 1. Zero temperature EOS for bcc Ta, LAPW GGA (●) and qEAM FF (——) results; energy (*a*) and pressure (*b*) as a function of volume.

3.1. EOS and elastic constants

The most important quantities used to develop the qEAM FF are zero temperature EOS for different crystal phases of Ta in a wide pressure range. We used energy–volume and pressure–volume data for bcc Ta from section 2; fcc–bcc energy difference and fcc pressure for different volumes from section 2; and first principles A15–bcc energy difference obtained by Söderlind and Moriarty [1] using full potential linear muffin-tin orbital method within the GGA approximation with spin–orbit interactions. Including the EOS of different phases (including metastable or unstable ones) in the FF development leads to an accurate description of the atomic interactions even when the environment of an atom is not that of the stable phase; this could play a key role in correctly describing the defects and non-equilibrium processes.

In figure 1, we show energy (figure 1(*a*)) and pressure (figure 1(*b*)) as a function of volume for bcc Ta at $T = 0$ K. The circles denote LAPW GGA results and the lines the qEAM FF. Figures 2 and 3 show energy–volume curves for fcc and A15 Ta, respectively. In figure 3, open circles show the A15 energy calculated by Söderlind and Moriarty [1], and the filled

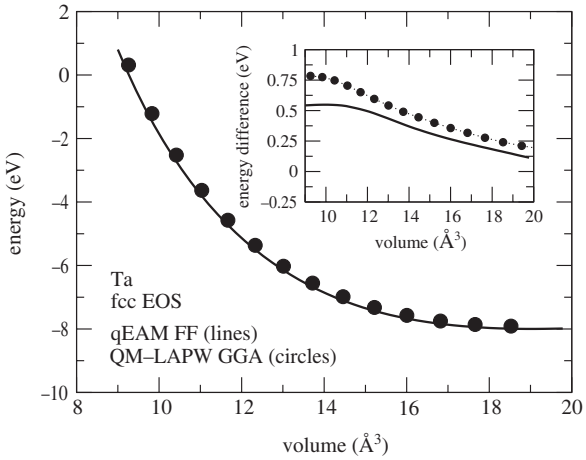

Figure 2. Zero temperature energy–volume curve for fcc Ta, LAPW GGA (●) and qEAM FF (——) results. The inset shows the fcc–bcc energy difference as a function of volume.

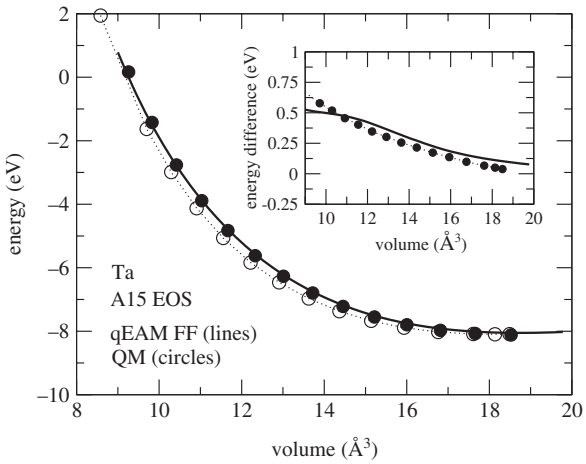

Figure 3. Zero temperature energy–volume curve for A15 Ta, *ab initio* (●, ○) and qEAM FF (——, · · · · · ·) results. Open circles with dotted lines denote full potential muffin-tin orbital calculation results [1]; filled circles show the sum of the A15–bcc energy difference from [1] and our calculation of bcc energy using the LAPW GGA method (section 2). The inset shows the A15–bcc energy difference as a function of volume (· · ●· · denote QM results [1] and the line qEAM FF).

circles denote the sum of the A15–bcc energy difference from [1] and our bcc energy from section 2; these are the quantities the FF was actually fitted to. The insets in figures 2 and 3 show the fcc–bcc and A15–bcc energy difference as a function of volume obtained with the qEAM FF (lines) and from QM (circles). In figure 4 we show the energy–volume curve for the hcp phase; circles denote the LAPW GGA results of section 2 and the lines show the qEAM FF results. Note that, although the hcp data was not included in the training set for the qEAM FF, the agreement is very good. Figures 1–4 show that the qEAM FF reproduces the zero temperature EOS for the four different phases very well. We have calculated the $T = 300\,\mathrm{K}$ EOS using isothermal–isobaric (NPT) MD with a Hoover [34] thermostat and

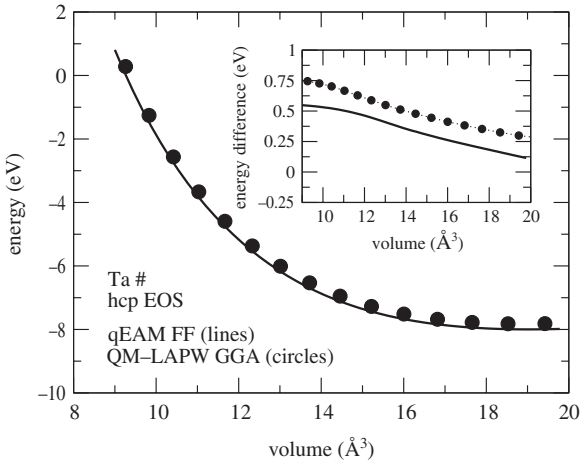

Figure 4. Zero temperature energy–volume data for hcp Ta, LAPW GGA (●) and qEAM FF (——) results. The inset shows the hcp–bcc energy difference as a function of volume.

Rahman–Parrinello barostat [35]. In table 1 we show the $T = 300$ K EOS parameters as well as recent compressibility data [26] obtained in a diamond-anvil cell at room temperature and ultrasonic measurements of adiabatic elastic constants [28].

We also included in the FF training set the *ab initio* elastic constants from section 2 at zero pressure. Table 1 shows bcc Ta EOS parameters (zero pressure volume (V_0), bulk modulus (B_T), its derivative with respect to pressure (B'_T) and the elastic constants) obtained using the qEAM FF together with the QM values from section 2 and the ones reported in [1]. V_0, B_T and B'_T were obtained by fitting Rose's universal EOS to the energy–volume data shown in figure 1.

In figure 5, we show the elastic constants (bulk modulus B_T, c_s, and c_{44}) as a function of pressure obtained with the qEAM FF (filled circles and full lines) and the LAPW results from section 2. While the agreement in B_T is excellent and that for c_s is good, qEAM FF greatly underestimates c_{44} for high pressures; this problem is amplified by the possible electronic phase transition that leads to a change of behaviour of c_{44} at ∼150 GPA (see section 2 and [27]).

3.2. Vacancy formation energy

We used experimental values for vacancy formation energy and cohesive energy in the training set used to fit the qEAM FF. The experimental value for the relaxed vacancy formation energy is $E_{vac} = 2.8$ eV [36]. From this value we estimated the value of the unrelaxed vacancy formation energy to be 3 eV. This unrelaxed value was used to fit the qEAM FF. The value for the cohesive energy used is $E_{coh} = 8.10$ eV [37].

The volume-relaxed vacancy formation energy is defined in computer simulations as: $e_{vac}(P) = e_{vac}(N-1, P) - ((N-1)/N)e_{xtal}(N, P)$, where $e_{xtal}(N, P)$ is the energy of the perfect crystal with N atoms at pressure P and $e_{vac}(N-1, P)$ is the energy corresponding to the $N-1$ atoms system with a vacancy at pressure P where the atomic positions are not allowed to relax. The relaxed vacancy formation energy is defined in the same way but with $e_{vac}(N-1, P)$ being the atom-relaxed energy of the system with a vacancy.

The volume-relaxed vacancy formation energy obtained using the qEAM FF is 3.10 eV, in very good agreement with the target value (3 eV) and only slightly lower than the *ab initio*

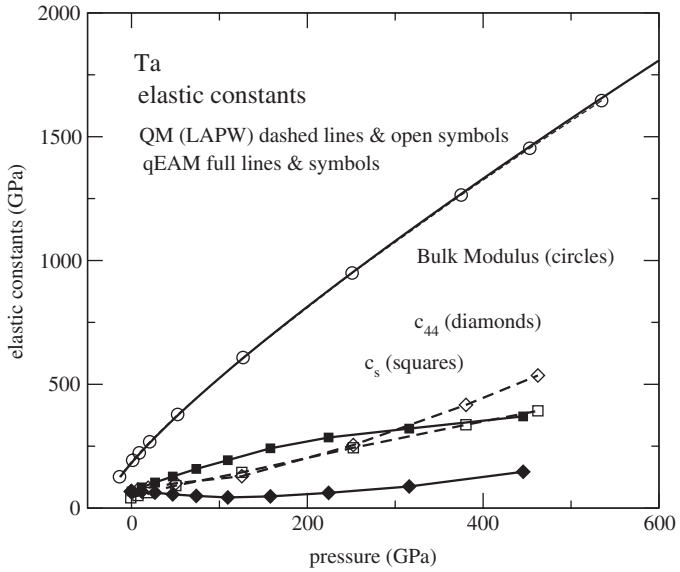

Figure 5. Zero temperature elastic constants for Ta, LAPW GGA (open symbols and dashed lines) and qEAM FF (filled symbols and full lines) results. Circles show bulk modulus; diamonds show c_{44} and squares represent $c_s = (c_{11} - c_{12})/2$.

Table 2. Volume-relaxed (e_{vac}^{vr}), full-relaxed vacancy formation (e_{vac}^{ar}), vacancy migration energies (e_{vac}^{mig}), and activation energy for self diffusion (Q).

	e_{vac}^{vr} (eV)	e_{vac}^{ar} (eV)	e_{vac}^{mig} (eV)	Q (eV)
		Theory (0 K)		
This work (qEAM FF)	3.10	2.935	1.093	4.028
This work (MB–PS)	3.25	—	—	—
FP LMTO GGA SC[a]	3.74	2.20	—	—
Plane waves LDA[b]	3.51	2.99	0.83	3.82
FP LMTO LDA[c]	3.49	—	—	—
		Theory and experiment (300 K)		
This work (qEAM FF)	—	3.0 ± 0.05	1.1 ± 0.05	4.1 ± 0.1
Experiment[d]	—	2.8 ± 0.6	—	3.8 ± 0.3

[a] Söderlind and Moriarty [2].
[b] Satta *et al* [3].
[c] Unrelaxed value by Korhonen *et al* [38].
[d] [36] for vacancy energy and [39] for activation energy.

value of 3.25 eV. The relaxed vacancy formation energy obtained with the qEAM FF is 2.95 eV, in good agreement with experiments. Table 2 summarizes our vacancy formation energies together with previous theoretical results and experimental data.

In figure 6(*a*) we show the volume-relaxed vacancy formation energy (e_{vac}) as a function of pressure (P) obtained with qEAM FF (thick solid line) and QM of section 2 (circles). We used a simulation cell containing 54 atoms for the perfect crystal case with periodic boundary conditions. Vacancy formation enthalpy is defined in the same way as $e_{vac}(P)$ replacing energy with enthalpy. In figure 6(*b*) we plot the vacancy formation enthalpy h_{vac} with respect to pressure. The difference between the vacancy formation enthalpy as obtained by qEAM

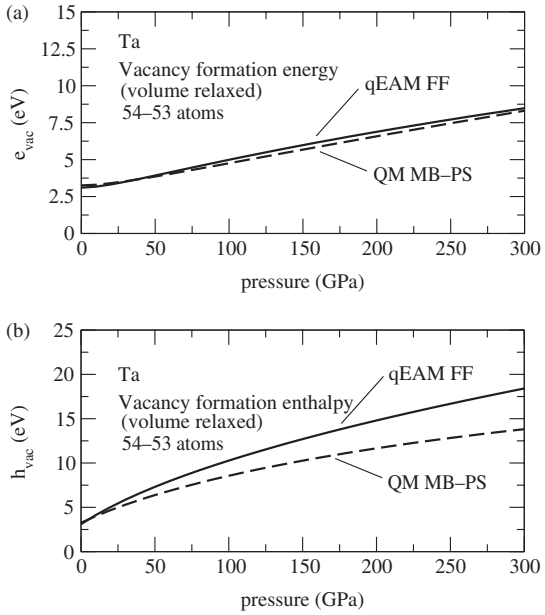

Figure 6. Volume-relaxed vacancy formation energy (*a*) and enthalpy (*b*) as function of pressure. Dashed lines represent *ab initio* MB–PS results (section 2) and full lines show qEAM results.

FF and QM, is due to the difference in the vacancy formation volume obtained by the two methods.

We calculated vacancy formation enthalpy at finite temperatures from NVT MD simulations at various volumes using a periodic unit cell with $N = 1458$ atoms. In figure 7, we show vacancy formation enthalpy as a function of pressure for $T = 0$ K (full atomic relaxation) and at $T = 300$ K (the volume-relaxed enthalpy is also shown for comparison); see also table 2 and the supplementary material [24].

A very important quantity, which determines vacancy mobility, is the vacancy migration energy barrier ($E_{\rm vac}^{\rm mig}$). We calculate $E_{\rm vac}^{\rm mig}$ using the qEAM FF by marching a nearest neighbour atom towards the position of the vacancy in short steps. At each step the position of the marching atom is fixed, as well as that of a distant, reference atom, and the positions of all the other atoms are relaxed at constant pressure. In this way, we obtain the optimum migration path and energy as a function of displacement. We obtain a vacancy migration energy $E_{\rm vac}^{\rm mig} \sim 1.093$ eV. The activation energy for self diffusion is defined as $Q = E_{\rm vac}^{f} + E_{\rm vac}^{\rm mig}$; using the qEAM FF we obtain $Q = 4.028$ eV in good agreement with the experimental value of 3.8 ± 0.3 eV [39], and *ab initio* calculations [3] which give 3.82 eV (see table 2). At $T = 300$ K we obtain a vacancy migration energy of 1.1 ± 0.5 eV (see table 2), very similar to the zero temperature value.

3.3. Energetics of homogeneously sheared bcc crystal

The ideal shear strength of a crystal is defined to be the stress separating elastic and plastic deformation when a homogeneous shear is applied to a perfect crystal. It gives an upper bound for the shear strength of the material. The shear transformation is in the direction of the observed twinning mode and deforms the crystal into itself [1, 40]. For the bcc crystal we use the transformation of the cell vectors as a function of shear value (s) defined in [1],

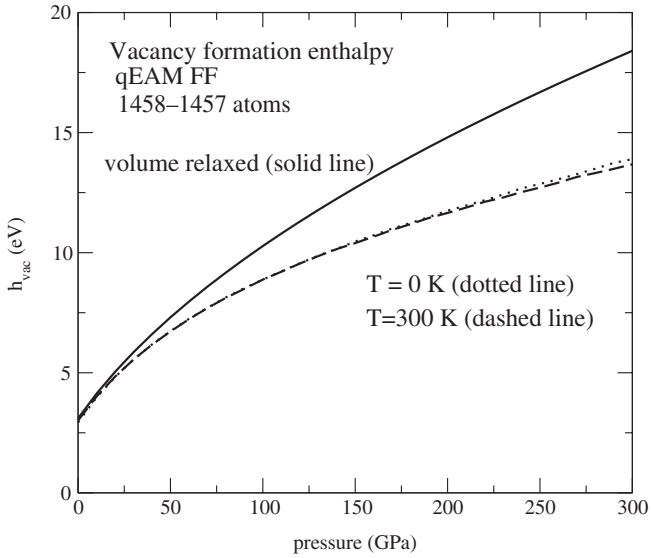

Figure 7. Vacancy formation enthalpy as function of pressure using the qEAM FF. The solid line shows the volume-relaxed result; dotted line, the $T = 0$ K fully relaxed results and the dashed line is $T = 300$ K result.

Table 3. Shear deformation in the observed twinning mode in Ta.

	This work (qEAM FF)		FP LMTO GGA SC[a]	
Volume (Å^3)	W_{max} (eV)	τ_{max}	W_{max} (eV)	τ_{max}
18.36	0.188	7.14	—	—
17.618 602	0.2	8.0	0.194	7.37
15.143 996	0.26	12.05	0.276	12.4
10.909 011 6	0.43	28.2	0.566	36.2

[a] Söderlind and Moriarty [1].

such that when s is equal to the twinning shear $s = s_{tw} = 2^{-1/2}$ the lattice vectors form a bcc structure, a twin of the initial one. In this way, we calculate the energy along the shear path: $W(s) = e(V, s) - e(V, s = 0)$, where $e(V, s)$ is the energy per atom of the deformed system and $e(V, s = 0)$ is the perfect crystal energy. The energy barrier associated with this transformation is $W_{max} = W(s = 0.5)$. The corresponding stress is defined as: $\tau(s) = (1/V)(\mathrm{d}W(s)/\mathrm{d}s)$. The ideal shear strength (τ_{max}) is defined as the maximum stress along the path.

In developing the qEAM FF we used QM calculations of W_{max} [1] for $V = 17.6186$ Å^3 and 10.909 Å^3 as part of the training set. In table 3 we compare the first principles results [1] and the ones obtained using the qEAM FF. We can see that the qEAM results are in very good agreement with the *ab initio* calculations.

3.4. Surface energy

The unrelaxed (100) surface energy using the qEAM FF is 1.971 J m^{-2}, lower than the first principles values of 3.097 J m^{-2} of [33] and 3.23 J m^{-1} of [41]. Low surface energy is a common problem in EAM-like FFs (see [12]). The zero temperature experimental estimate of the surface energy (averaged over different surfaces) is 2.902 J m^{-2} [42].

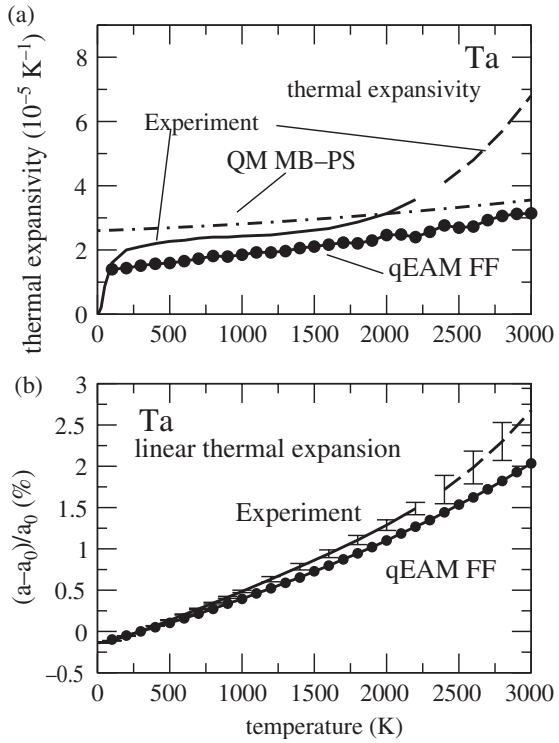

Figure 8. Thermal expansion in Ta. (*a*) Thermal expansivity as a function of temperature; circles represent qEAM FF results, the dash-dotted lines shows QM results and the line denotes experimental results from [45]. (*b*) Linear thermal expansion of Ta; $(a - a_0)/a_0$ as a function of temperature; circles represent qEAM FF results and the line denotes experimental results from [45]. The high temperature experimental data (- - - -) are provisional values [45].

4. Thermal expansion

Thermal expansivity is an important materials property that can be calculated directly from MD simulations. We calculate the lattice constant as a function of temperature for zero pressure using NPT MD, with a computational cell containing 1024 atoms, increasing the temperature by 100 K every 25 ps at zero applied pressure. For each temperature the first 5 ps were taken as thermalization and the remaining 20 ps were used for measurements [24]. *Ab initio* MD simulations are very time consuming and only feasible for small systems and short times; thus, in order to calculate the thermal expansion from first principles we compute the electronic contribution to the free energy using quantum statistical mechanics and the vibrational part is obtained using the particle in a cell method [44]. Further details of our calculations can be found in [43]. These calculations were performed using the mixed basis pseudopotential method and a cell containing 54 atoms.

Figure 8(*a*) shows the thermal expansivity ($\alpha(T) = (1/V)(\partial V/\partial T)$) as a function of temperature obtained from our MD simulations (circles), first principles results (dash-dotted line), as well as the experimental values (full and dashed lines) [45]. Figure 8(*b*) shows the linear thermal expansion $(a - a_0)/a_0$ (where a_0 is the $T = 300$ K lattice constant) as a function of temperature obtained using the qEAM FF (circles) as well as the experimental values [45]. The high temperature experimental results (shown as dashed lines) represent provisional experimental data [45]. Both MD and the particle in cell methods are based on

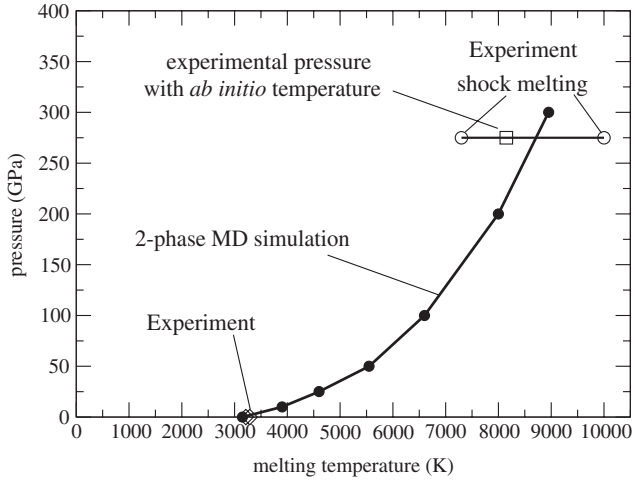

Figure 9. Ta melting qEAM FF; melting curve for Ta up to $P = 300$ GPa obtained using the two-phase simulation technique. We also show the experimental zero pressure melting temperature [46] (●, ○) and the results of shock melting [48].

classical mechanics so none of them are expected to capture the low temperature behaviour where the differences between quantum and classical statistical mechanics are important. The FF results agree with experimental data well; e.g. the qEAM FF underestimates the change in lattice parameter from $T = 300$ to 2000 K by less than 0.2%. This is an important result since the thermal expansion in related to anharmonicities of the internal energy. Our *ab initio* data also agree well with the experimental results; we slightly overestimate thermal expansivity for temperatures lower than $T = 2000$ K.

5. Melting curve of Ta

We studied melting of Ta using two-phase MD simulations with the qEAM FF. We place pre-equilibrated liquid and solid samples in a single computational cell. Once this initial configuration is built we perform a NPT MD (Nos"é"-Hoover thermostat and Rahman–Parinello barostat) simulation and observe which phase grows. If the simulation temperature T is lower than the melting temperature at the given pressure ($T_{\rm melt}(P)$) the liquid will start crystallizing; on the other hand, the solid will melt if $T > T_{\rm melt}(P)$. At zero pressure we find the melting temperature to be $T = 3150 \pm 50$ K. This value for the zero pressure melting point is in very good agreement with experimental results, which range from 3213 to 3273 K [46]. This is a very important validation of the FF, taking into account that only zero temperature data were used in its development. Using the Clausius Clapeyron equation we calculate the slope of the melting curve at zero pressure to be $\mathrm{d}T/\mathrm{d}P = 92.8\,\mathrm{K\,GPa^{-1}}$, larger than the experimental value $\mathrm{d}T/\mathrm{d}P = 60 \pm 10\,\mathrm{K\,GPa^{-1}}$ [47].

Using the two phase simulation procedure we calculated the melting temperature for various pressures up to 300 GPa. Figure 9 shows the melting curve for Ta (see also [24]). To the best of our knowledge, this is the first calculation of melting temperature in Ta for such a wide pressure range. Zero pressure experimental values [46] are also shown in figure 9 as empty diamonds. High pressure melting of Ta has been studied experimentally via shock compression [48]; melting is identified as a change in the velocity of the rarefaction wave (from the longitudinal to the bulk sound velocity). The transition was found to occur in the

pressure range from ∼250 to 295 GPa [48]. The calculation of the temperature in shock experiments (i.e. along the Hugoniot) is difficult; the electronic contribution to the specific heat has a very strong effect on the melting temperature [48]. Simple models for the electronic behaviour lead to very different temperatures: using the free electron gas model, the melting temperature is ∼10 000 K while considering band electrons gives $T_{\rm melt} \sim 7500$ K (see [48]). These experimental values are shown in figure 9 as empty circles. Using the accurate *ab initio* thermal EOS obtained using the methods described above and the Rankine–Hugoniot equation, Cohen and Gülseren calculated pressure–volume and temperature–pressure curves for Ta under shock conditions [43]. This calculation leads to a melting temperature (using the experimental melting pressure $P_{\rm melt} = 375$ GPa) of 8150 K (squares in figure 9). Our MD results are in good agreement with the high pressure calculation of the melting temperature based on shock experiments and *ab initio* calculations. Recent experiments using laser heating on diamond anvil cells [56] lead to a much weaker dependence of melting temperature with pressure (leading to zero slope at ∼40 GPa) than our calculations and the one implied by the shock data.

6. Conclusions

We have derived an accurate classical FF for Ta based on extensive *ab initio* QM calculations and used it with MD to calculate finite temperature properties. The large amount of QM data used to derive our FF gives an important measure of its overall quality. The behaviour of the elastic c_{44} with pressure (a dependence very rarely tested for interatomic potentials) and recent comparison between qEAM forces with *ab initio* ones [17] indicate there is room for improvement (the lack of angular terms in EAM is known to limit its ability to describe bonding between partially filled d orbitals). While the new EAM potential by Li *et al* reproduces *ab initio* forces (to which it was fitted) more accurately than qEAM, our potential shows a better description of the thermal expansivity. Also, the accurate description of the maximum theoretical shear strength may play an important role in the description of phenomena relevant to plasticity such as the Peierls stress and generalized stacking fault [49].

We used the qEAM FF with MD to calculate the melting curve for Ta in a wide pressure range. The zero pressure melting temperature obtained from our simulations $T_{\rm melt} = 3150 \pm 50$ K is in very good agreement with the experimental result of 3290 ± 100 K. This is an important validation of our approach given the fact that the qEAM FF was derived using zero temperature data.

First-principles-based FFs represent an important step in *ab initio* multiscale modelling of materials. We have used the qEAM FF to study spall failure [50], crack propagation, and dislocation properties such as core structure and energy, mobility (see [51] in this issue and [49, 52]), and kink formation energies [53]. There has been some debate regarding the ability of EAM-type FFs to correctly describe the core structure of screw dislocations in bcc metals. We have recently shown that qEAM type FFs, if carefully parametrized, can correctly describe the core structure as well as mobility of screw dislocations in Ta [49]. These first-principles-based calculations of the fundamental mechanisms that govern the mechanical properties of materials have been used with a micromechanical model of plasticity developed by Stainer and co-workers [54] to predict single crystal plasticity in Ta [55].

Acknowledgments

This research was funded by a grant from DOE-ASCI-ASAP (DOE W-7405-ENG-48). The facilities of the MSC are also supported by grants from NSF-CHE, ARO-MURI, ARO-DURIP,

NIH, ChevronTexaco Corp., Seiko Epson, General Motors, Asahi Kasei, and Beckman Institute. Thanks to D Singh and H Krakauer for use of their LAPW code. We also thank P Söderlind and J Moriarty for providing us with LMTO data. Computations were partially performed on the Cray SV1 at the Geophysical Laboratory, supported by NSF grant EAR-9975753 and the W M Keck Foundation.

References

[1] Söderlind P and Moriarty J A 1998 *Phys. Rev.* B **57** 10340
[2] Söderlind P, Yang L H, Moriarty J A and Wills J M 2000 *Phys. Rev.* B **61** 2579
[3] Satta A, Willaime F and de Gironcoli S 1999 *Phys. Rev.* B **60** 7001
[4] Ismail-Beigi S and Arias T A 2000 *Phys. Rev. Lett.* **84** 1499
Woodward C and Rao S I 2002 *Phys. Rev. Lett.* **88** 216402
Segall D E, Strachan A, Goddard III W A, Ismail-Beigi S and Arias T A 2003 *Phys. Rev.* B **68** 014104
[5] Moriarty J A 1994 *Phys. Rev.* B **49** 12431
[6] Xu W and Moriarty J A 1996 *Phys. Rev.* B **54** 6941
[7] Moriarty J A, Xu W, Söderlind P, Belak J, Yang L H and Zhu J 1999 *J. Eng. Mater. Tech.* **121** 120
[8] Daw M S and Baskes M I 1983 *Phys. Rev. Lett.* **50** 1285
Daw M S and Baskes M I 1984 *Phys. Rev.* B **29** 6443
[9] Foiles S M, Baskes M I and Daw M S 1986 *Phys. Rev.* B **33** 7983
[10] Chantasiriwan S and Milstein F 1996 *Phys. Rev.* B **53** 14080
[11] Johnson R A and Oh D J 1989 *J. Mater. Res.* **4** 1195
[12] Guellil A M and Adams J B 1992 *J. Mater. Res.* **7** 639
[13] Ercolessi F and Adams J B 1994 *Europhys. Lett.* **26** 583
[14] Payne M C, Robertson I J, Thomson D and Heine V 1996 *Phil. Mag.* B **73** 191
[15] Strachan A, Çağın T and Goddard III W A 1999 *Phys. Rev.* B **60** 15084
[16] Mishin Y, Karkas D, Mehl M J and Papaconstantopoulos D A 1999 *Phys. Rev.* B **59** 3393
[17] Li Y, Siegel D J, Adams J B and Liu X-Y 2003 *Phys. Rev.* B **67** 125101
[18] Baskes M I 1987 *Phys. Rev. Lett.* **59** 2666
Baskes M I, Nelson J S and Wright A F 1989 *Phys. Rev.* B **40** 6085
[19] Baskes M I 1992 *Phys. Rev.* B **46** 2727
Lee B-J, Baskes M I, Kim H and Cho Y K 2001 *Phys. Rev.* B **64** 184102
[20] Wei S H and Krakauer H 1985 *Phys. Rev. Lett.* **55** 1200–3
[21] Singh D J 1994 *Planewaves, Pseudopotentials, and the LAPW Method* (Boston: Kluwer)
[22] Perdew J P, Kieron Burke and Matthias Ernzerhof 1996 *Phys. Rev. Lett.* **77** 3865
[23] Monkhorst H J and Pack J D 1976 *Phys. Rev.* B **13** 5188
[24] See our web site, http://www.wag.caltech.edu/publications/papers/
[25] Vinet P, Ferrante J, Smith J R and Rose J H 1986 *J. Phys. C: Solid State Phys.* **19** L467
Vinet P, Rose J H, Ferrante J and Smith J R 1987 *J. Phys.: Condens. Matter* **1** 1941
[26] Cynn H and Yoo C-S 1999 *Phys. Rev.* B **59** 8526
[27] Gülseren O and Cohen R E 2001 *Phys. Rev.* B **63** 224101
[28] Katahara K W, Manghnani M H and Fisher E S 1979 *J. Phys. F: Metal Phys.* **9** 773
Katahara K W, Manghnani M H and Fisher E S 1976 *J. Appl. Phys.* **47** 434
[29] Cohen R E, Gülseren O and Hemley R J 2000 *Am. Mineral.* **85** 338–44
[30] Mukherjee S, Gülseren O and Cohen R E unpublished
[31] Gülseren O, Bird D M and Humphreys S E 1998 *Surf. Sci.* **402–404** 827
[32] Perdew J P and Wang Y 1992 *Phys. Rev.* B **46** 6671
[33] Vitos L, Ruban A V, Skriver H L and Koll'ar J 1998 *Surf. Sci.* **411** 186
[34] Hoover W G 1985 *Phys. Rev.* A **31** 1695
[35] Parinello M and Rahman A 1981 *J. Appl. Phys.* **52** 7182
[36] Maier K, Peo M, Saile B, Schaefer H E and Seeger A 1979 *Phil. Mag.* A **40** 701
[37] de Boer F R *et al* 1988 *Cohesion in Metals: Transition Metal Alloys* (New York: Elsevier)
[38] Korhonen T, Puska M J and Nieminen R M 1995 *Phys. Rev.* B **51** 9526
[39] Weiler D, Maier K and Mehrer H 1983 *Diffusion in Metals and Alloys* ed F J Kedves and D L Beke (Aedermannsdorf: Trans Tech Publications)
[40] Paxton A T, Gumbsch P and Methfessel M 1991 *Phil. Mag. Lett.* **63** 267
[41] Christine Wu, Yang L H, Klepeis J E and Mailhiot C 1995 *Phys. Rev.* B **52** 11784

[42] Tyson W R and Miller W A 1977 *Surf. Sci.* **62** 267
[43] Cohen R E and Gulseren O 2001 *Phys. Rev.* B **63** 224101
[44] Holt A C, Hoover W G, Gray S G and Shortle D R 1970 *Physica* **49** 61
Ree F H and Holt A C 1973 *Phys. Rev.* B **8** 826
Westera K and Cowley E R 1975 *Phys. Rev.* B **11** 4008
Cowley E R, Gross J, Gong Z and Horton G K 1990 *Phys. Rev.* B **42** 3135
[45] Touloukian Y S, Kirby R K, Taylor R E and Desai P D 1975 *Thermophysical Properties of Matter (Thermal Expansion—Metallic Elements and Alloys)* vol 12 (New York: Plenum)
[46] Hultgren R, Desai P D, Hawkins D T, Gleiser M, Kelley K K and Wagman D D 1973 *Selected Values of the Thermodynamical Properties of the Elements* (Metals Park, OH: American Society for Metals)
[47] Shaner J W, Roger Gathers G and Minichino C 1977 *High Temp.—High Pressures* **9** 331
[48] Brown J M and Shaner J W 1984 *Shock Waves in Condensed Matter-1983* ed J R Asay *et al* (New York: Elsevier)
[49] Wang G, Strachan A, Çağın T and Goddard III W A 2003 *Phys. Rev.* B **67** 140101
[50] Strachan A, Çağın T and Goddard III W A 2001 *Phys. Rev.* B **63** 060103(R)
[51] Wang G, Strachan A, Çağın T and Goddard III W A 2004 *Modelling Simul. Mater. Sci. Eng.* **12**
[52] Wang G, Strachan A, Çağın T and Goddard III W A 2001 *Mater. Sci. Eng.* A **309** 133
[53] Wang G, Strachan A, Çağın T and Goddard III W A *Phys. Rev.* B submitted
[54] Cuitiño A M, Stainer L and Ortiz M 2000 *J. Mech. Phys. Solids* **50** 1511
[55] Cuitiño A M, Stainier L, Wang G, Strachan A, Çağın T, Goddard III W A and Ortiz M 2002 *J. Comput. Aided Mater. Des.* **8** 27
[56] Errandonea D *et al* 2001 *Phys Rev.* B **63** 132104